Peer reviewed version

Link to published version (if available):
[10.1109/RadarConf2147009.2021.9455175](#)

[Link to publication record in Explore Bristol Research](#)
PDF-document

University of Bristol - Explore Bristol Research
General rights

UWB and WiFi Systems as Passive Opportunistic Activity Sensing Radars

Mohammud J. Bocus*, Kevin Chetty†, Robert J. Piechocki*

*Department of Electrical and Electronic Engineering, University of Bristol, UK

†Department of Security and Crime Science, University College London, UK

{junaid.bocus,r.j.piechocki}@bristol.ac.uk, k.chetty@ucl.ac.uk

Abstract—Human Activity Recognition (HAR) is becoming increasingly important in smart homes and healthcare applications such as assisted-living and remote health monitoring. In this paper, we use Ultra-Wideband (UWB) and commodity WiFi systems for the passive sensing of human activities. These systems are based on a receiver-only radar network that detects reflections of ambient Radio-Frequency (RF) signals from humans in the form of Channel Impulse Response (CIR) and Channel State Information (CSI). An experiment was performed whereby the transmitter and receiver were separated by a fixed distance in a Line-of-Sight (LoS) setting. Five activities were performed in between them, namely, sitting, standing, lying down, standing from the floor and walking. We use the high-resolution CIRs provided by the UWB modules as features in machine and deep learning algorithms for classifying the activities. Experimental results show that a classification performance with an F1-score as high as 95.53% is achieved using processed UWB CIR data as features. Furthermore, we analysed the classification performance in the same physical layout using CSI data extracted from a dedicated WiFi Network Interface Card (NIC). In this case, maximum F1-scores of 92.24% and 80.89% are obtained when amplitude CSI data and spectrograms are used as features, respectively.

I. INTRODUCTION

Recently, Human Activity Recognition (HAR) using device-free methods has become a reality with the proliferation of wireless devices in both residential and commercial environments. These methods, which are mostly based on Radio-Frequency (RF) sensing, can provide an automated, inexpensive and non-invasive solution for use in surveillance to predict criminal activities in public places, vehicular technology and in other scenarios that involve human and machine interaction [1]. Furthermore, over the past few decades, there have been increasing concerns related to health issues such as mental health problems, cardiovascular diseases, Alzheimer's, strokes among many others. Activity sensing can provide insightful information related to pattern-of-life and can be used to monitor a patient's health in terms of inactivity or falls. These indicators can then be used to identify chronic diseases or any other health issues for which early treatment interventions are critical [2]. This has inspired a number of research to be carried out for automated human activity and behaviour sensing using technological devices such as wearable sensors [3] and camera-based systems [4].

On the other hand, device-free passive sensing using RF waves provides a better alternative since the users or patients do not have to face any discomfort by wearing devices on their body. Moreover, passive sensing systems do not breach the user's privacy compared to camera-based systems and also, they are not sensitive to lighting conditions and physical obstacles do not pose a problem. In addition to these benefits, wireless systems such as WiFi are found in almost all residential and commercial indoor environments nowadays. These devices are also inexpensive and they do not require additional infrastructure for passive wireless sensing.

Ultra-wideband (UWB) is another wireless communication technology that has been used over the years for providing ranging and positioning with centimetre-level accuracy. The main features of this technology include a wide frequency bandwidth ($\geq$ 500 MHz) to provide high localisation accuracy, high immunity against multipath phenomenon and interference and low output power [5]. UWB systems are used extensively in industry where manual operations have been replaced by automated machineries and hence it is vital to track these systems to ensure their proper functioning. This technology can also be used to locate tagged assets in factories and warehouses or track medical personnel in a hospital, among many other applications.

In this work, we make the following contributions:

- Very limited work has been performed regarding HAR using UWB technology. Therefore, in this paper we present the techniques and address the feasibility of using UWB signals for HAR.
- We extract high-resolution Channel Impulse Responses (CIRs) from UWB modules and use them as features in machine/deep learning algorithms for classifying the different human activities.
- We also compare the activity classification performance using fine-grained WiFi Channel State Information (CSI) in the same physical layout .

The rest of the paper is organised as follows. The related works on HAR using WiFi CSI and UWB signals are given in Section II. Section III describes the system models for UWB and WiFi CSI. Section IV presents the signal processing techniques applied to the UWB and WiFi CSI signals for activity sensing. The performance evaluation of the two systems is investigated in Section V in terms of activity classification accuracy using machine and deep learning algorithms. Finally, conclusions are drawn at the end of this paper.

II. RELATED WORK

The granularity of the information provided by RF signals, such as those emitted from WiFi, may be used for different applications. For instance, [6] leverages the fluctuations in the coarse-grained Received Signal Strength Indicator (RSSI) from a single Access Point (AP) to detect in-air hand gestures around the user's mobile device with an accuracy of 87.5%. The downside of RSSI is that it is vulnerable to multipath fading and has a tendency to fluctuate over time, even in a non-dynamic environment. Hence, recent studies have considered the fine-grained CSI extracted from WiFi signals for various applications such as HAR [7]–[9], fall detection [10], gait [11], gesture [12], [13] and sign recognition [14], intrusion detection [15] and crowd-counting [16]. The work in [8] achieved a high activity recognition accuracy ($\approx$96%) for activities such as sitting, walking and falling down by using the time-frequency features of the WiFi CSI signals. The authors of [11] used torso and limb velocities, derived from the information obtained in CSI spectrograms, to detect a walking human with an accuracy of 92% at a distance of 14 m. While there are numerous studies on HAR using WiFi CSI, it is not the case for UWB technology. The latter has been designed for localisation, positioning or tracking purposes. Since UWB chips are commercially available, a number of research studies have been carried out to test this technology in various scenarios in terms of localisation and ranging but very limited research has been dedicated to activity recognition using UWB signals. For instance, the authors of [17] proposed to use the CIR data extracted from the UWB signals for HAR. They achieved a classification accuracy as high as 95% for simple activities such as sitting, standing and laying down using machine learning algorithms.

III. SYSTEM MODELS

A. DW1000 Specifications

In the experiment, two Decawave's EVK1000 evaluation boards are used. Each board consists of a DW1000 chip, ARM Cortex M3 microcontroller, LCD display, USB interface and an off-board antenna. The evaluation kit is based on the 802.15.4a standard and it uses the Two-Way Ranging (TWR) protocol to provide accurate distance measurements. The EVK1000 board provides various modes of operation such that the user can choose between different carrier frequencies (from 3.5 to 6.5 GHz), bandwidths (500 MHz and 900 MHz), data rates (110 kbps, 850 kbps or 6.81 Mbps), Pulse Repetition Frequency (PRF) of 16 MHz or 64 MHz, and preamble lengths from 64 to 4096 symbols [18].

B. UWB Channel Impulse Response (CIR)

The IEEE 802.15.4 frames consist of preambles. The DW1000 chip estimates the CIR by correlating a known preamble sequence with the received signal and accumulating the result over a period of time [19]. The CIR $h(t)$ characterises the multipath propagation between the transmitter and receiver and is represented as

$$h(t) = \sum_{p=0}^{P-1} \alpha_p \delta(t - \tau_p), \tag{1}$$

where P is the number of paths in the multipath channel, α_p and τ_p denote the amplitude and delay of the pth path, respectively. The CIR is stored in the accumulator of the DW1000 chip and it spans one symbol period. This represents 1016 and 992 samples for the nominal 64 MHz and 16 MHz PRFs, respectively [18]. Each sample is made up of a 16-bit real integer and a 16-bit imaginary integer and the sampling interval is equal to $1/(2 \times 499.2 \text{ MHz}) \approx 1.0016$ ns. Since an UWB system has a high multipath resolution capability, the Time-of-Flight (ToF) of the first path, τ_0, can easily be identified and the distance, d, between the transmitter and receiver can simply be computed as

$$d = c \times \tau_0, \tag{2}$$

where c is the speed of light ($\approx 3 \times 10^8$ m/s).

C. WiFi CSI System

In this work, we extract the CSI from an Intel 5300 chipset using the Linux CSI tool [20] which is based on the IEEE 802.11n standard. In a WiFi system based on the Orthogonal Frequency Division Multiplexing (OFDM) physical layer waveform, the channel bandwidth is shared among multiple orthogonal and overlapping subchannels which carry the data in a wireless channel. When a signal is transmitted through a wireless channel, it suffers from various propagation phenomena such as multipath fading, attenuation, scattering, phase shift, etc. In order to ensure reliability of the communication link and recover the transmitted data, the receiver needs to estimate the channel. Similar to the UWB system which uses preambles to estimate the CIR, the WiFi system also sends pilot symbols on specific OFDM subcarriers, which are known by both the transmitter and receiver, through the wireless medium. This process is also known as channel sounding. The receiver basically uses the known transmitted and received pilot symbols to compute the channel estimates (i.e., CSI) as complex-valued coefficients in the frequency domain. The equaliser then uses the CSI to reverse the effects of the channel and recover the transmitted data. For a Wi-Fi system with Multiple-Input Multiple-Output (MIMO) OFDM capability, the CSI in each received packet is obtained as a 3-dimensional (3D) matrix with $n_t \times n_r \times N$ complex values, where n_t is the number of transmit antennas, n_r is the number of receive antennas and N is the number of subcarriers. For a given packet, the CSI for the kth subcarrier can be represented as

$$\mathbf{H}_k = \begin{bmatrix} h_{1,1} & h_{1,2} & \cdots & h_{1,n_t} \\ h_{2,1} & h_{2,2} & \cdots & h_{2,n_t} \\ \vdots & \vdots & \ddots & \vdots \\ h_{n_r,1} & h_{n_r,2} & \cdots & h_{n_r,n_t} \end{bmatrix}, \tag{3}$$

where $h_{i,j}$ is the complex-valued channel coefficient between the jth transmit antenna and ith receive antenna. Using the tool in [20], CSI can be extracted over only 30 subcarriers in the 20/40 MHz channel bandwidths for both the 2.4 GHz and 5 GHz bands.
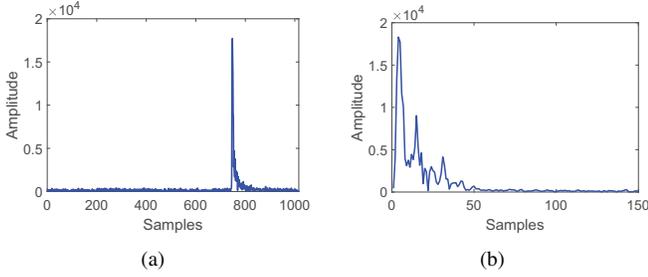
Fig. 1. (a) Raw CIR (1016 samples) and (b) CIR after denoising (150 samples).

IV. Signal Processing for Activity Sensing

A. UWB

For the UWB system, we use the high-resolution CIRs as features for activity classification using machine/deep learning algorithms. However, before proceeding with this step, the raw CIR is denoised, where the samples before the first peak in Fig. 1(a) are considered as noise and removed and the 150 subsequent samples as from the first peak are retained to obtain the processed CIR in Fig. 1(b). This pre-processing step also reduces the dimensionality of the data, thereby decreasing the computational complexity of the system. In order to show how the activities affect the UWB signals, we convert the raw CIR signal (1016 samples) to the frequency domain using Fast Fourier Transform (FFT) and the resultant signal is known as the Channel Frequency Response (CFR). Fig. 2 shows the signals recorded for the five different activities in terms of CFR amplitude versus time duration for one frequency sample out of the 1016 samples. As can be observed in Fig. 2, the UWB signals are free from environmental noise or interference and hence do not require denoising in this domain. On the other hand, the raw WiFi CSI signals are much noisier in nature due to the WiFi channels being overcrowded and hence they are susceptible to a lot of interference and environmental noise, in addition to electrical noise in the hardware. Therefore, some filtering or denoising techniques need to be applied to obtain clean signals. This will allow the classification algorithms to learn the patterns in the signals more efficiently. From Fig. 2, it can be observed that each activity results in a distinct pattern that can be easily distinguished from each other.

B. WiFi CSI

The signal processing techniques that are applied to the raw CSI data for the purpose of HAR are described next.

1) Noise Filtering: The raw CSI values that are measured are inherently noisy. The noise reduction process is an important step to minimise the impact of environmental factors in the monitoring area such as interference or variations in the signal due to moving objects or people in the vicinity [17]. For de-noising the WiFi CSI data, we utilise the Discrete Wavelet Transform (DWT) technique for filtering in-band noise while preserving the high frequency components to prevent the signal from being distorted. This technique transforms the signal into the wavelet domain by passing it through a number of lowpass and highpass filters which provide the
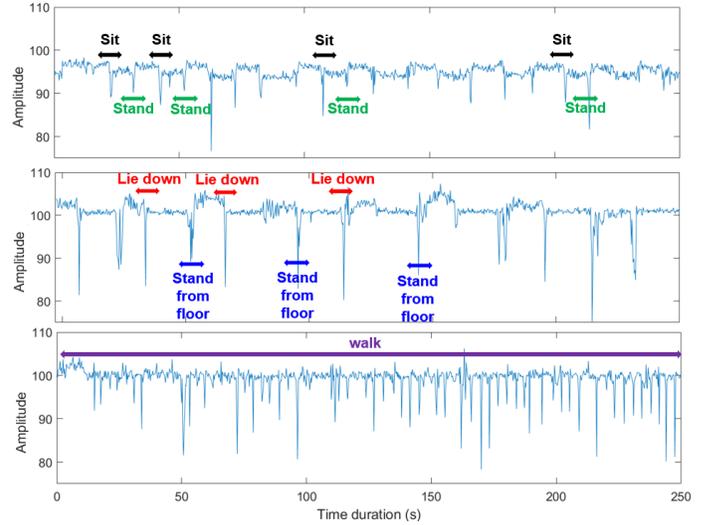

Fig. 2. Raw UWB signals for five activities (CFR amplitude versus time duration).
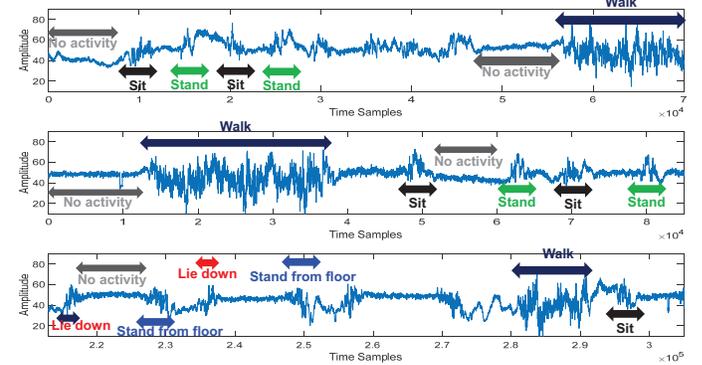

Fig. 3. Filtered WiFi CSI signals.

approximation and detailed coefficients, respectively [10]. The detailed coefficients in the first level hold information about the noise and the abrupt changes as a result of human activities. These coefficients are used to compute a threshold which is adapted for lower wavelets and the noise is eliminated in all levels without significantly distorting the signal. Fig. 3 shows the denoised WiFi CSI signals for different measurements which cover the five activities. As can be observed, the CSI measurements across the received packets capture the changes in the wireless signal due to the latter's interaction with the human activities. The signals show distinct patterns for each activity and therefore after the activity segmentation step, the resultant signals can be directly fed to a classification algorithm or retained for further processing [7].

2) Activity Segmentation: The variations in the signal due to a given activity can be segmented using the Moving Variance Segmentation (MVS) [21] approach. The key idea behind this technique is to compute, in a stepwise fashion, the moving variance in the CSI stream like the one shown in Fig. 4(a). Basically, in each step, a moving variance is computed over a sliding window of length L across neighbouring CSI samples, and the window is centred about the CSI sample in the current position. The moving variance for a CSI stream
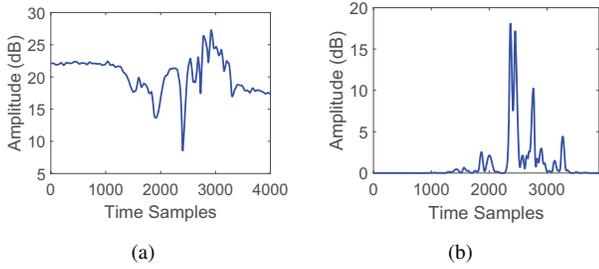
Fig. 4. MVS for standing activity (a) CSI stream (b) Corresponding moving variance sequence.
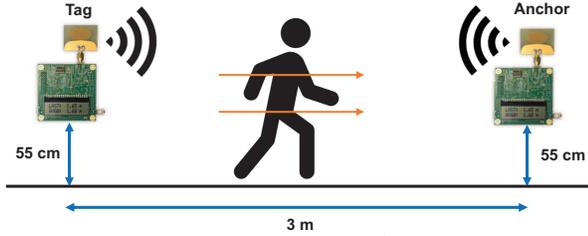

Fig. 5. Experiment Layout for HAR.

which consists of M packets is computed as [21]

$$\text{CSI}_{\text{mv}} = \sum_{m=1}^{M} \left[\frac{1}{L-1} \sum_{l=1}^{L} |\text{CSI}_{l \in L} - \mu^2| \right], \qquad (4)$$

$$\mu = \frac{1}{L} \sum_{l=1}^{L} \text{CSI}_l,$$

where μ and l denote the mean and packet number in the sliding window of length L, respectively, and m is the current sample position in the CSI stream. The CSI stream in Fig. 4(a) corresponds to the variations in the signal due to the standing up activity and its corresponding moving variance stream is shown in Fig. 4(b), where a sliding window of length $L = 100$ has been chosen to achieve the best results. As can be observed in Fig. 4(b), the variations in the signal due to human motion result in high moving variance values while slight fluctuations such as those obtained in a static environment, result in smaller values. Using the MVS method, the start and end points of an activity can be easily identified and therefore segmentation can be performed to remove undesired samples and consequently improve the system's performance [7].

3) Data Size Reduction: In this experiment, an AP sent data across one transmit antenna ($n_t = 1$) and CSI was extracted at the receiver over three antennas ($n_r = 3$). For this setup, $1 \times 3 \times 30 = 90$ complex CSI values are obtained in each packet. A packet rate of 1 kHz was considered and this results in significant amount of data that needs to be processed [7]. Therefore, in this work we consider the Principal Component Analysis (PCA) technique for reducing the dimensionality of the CSI data, thereby decreasing the computational complexity. PCA identifies the time-varying correlations between the CSI waveforms which are then optimally combined to obtain components that represent the variations due to human activities [22]. We extract the first six principal components but discard the first one since it contains noise due to reflection from stationary objects like walls, furniture, etc., and therefore
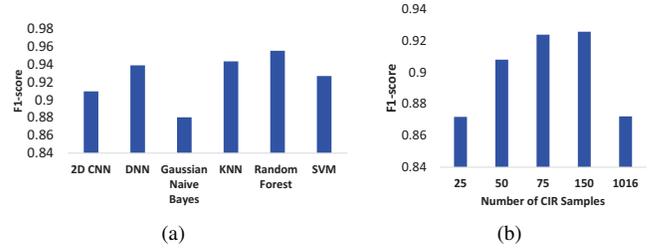

Fig. 6. (a) Classification performance using UWB CIR (150 samples) as features (b) Impact of the number of CIR samples on classification performance.

discarding it will not result in any loss of information [8], [11], [16].

4) Time-Frequency Analysis (using spectrograms): The CSI data is sensitive to changes in the monitoring area such that the signals which are reflected from the human body result in different frequencies when various activities are performed [7]. The change of frequencies over time can be identified by applying the Short-time Fourier Transform (STFT) to the CSI signal. The basic idea behind STFT is to apply a sliding window to the signal to obtain equally-sized segments and then FFT is applied to the samples in each segment. The window size selected for the FFT determines the trade-off between time and frequency resolutions. A large window size results in a high frequency resolution but low time resolution, and vice versa.

V. PERFORMANCE EVALUATION

A. System Description

The UWB CIR and WiFi CSI data collection was carried out in a monitoring area of dimension 4 m × 5 m with furniture and other objects in the surroundings. As shown in Fig. 5, one EVK1000 board is configured as an anchor (receiver) while the other is configured as a tag (transmitter). Since HAR is the main focus of this study, the two boards were kept fixed at a separation distance of 3 m in a Line-of-Sight (LoS) setup and 5 activities were performed between them, namely, sitting, standing, walking, lying down and standing from the floor. It should be noted that the activities were performed in different orientations in a natural way, as would be the case in the real world. The two boards were configured in Mode 3, which specifies a bandwidth of 500 MHz for a carrier frequency of 4.0 GHz, PRF of 64 MHz, preamble length of 1024 and data rate of 110 kbps. The anchor was connected to a laptop and CIR data was logged for offline processing.

The WiFi CSI was extracted using the Linux 802.11n [20] tool which was also stored for offline processing. The transmitter was a TP-Link AP transmitting data with one antenna while the receiver was an Intel Next Unit of Computing (NUC) device equipped with the Intel 5300 Network Interface Card (NIC) from which CSI is extracted from 30 out of 56 subcarriers for each transmit-receive antenna pair. The CSI data was collected over 3 receiving antennas in the 5 GHz band (40 MHz bandwidth) by pinging the AP at a rate of 1000 packets/s. This rate was chosen to capture
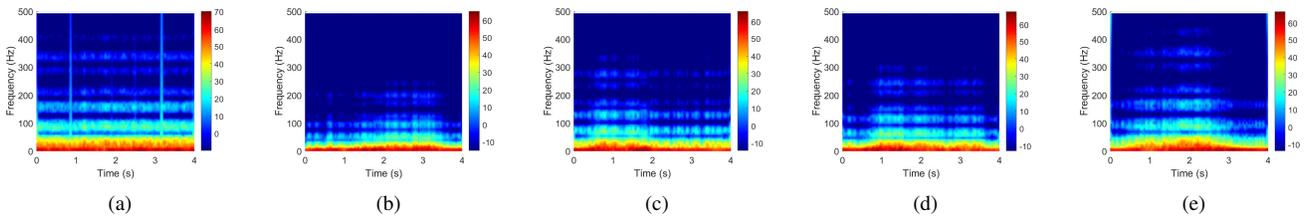
Fig. 7. WiFi CSI spectrograms: (a) walk, (b) sit, (c) stand, (d) lay down, (e) stand from floor.
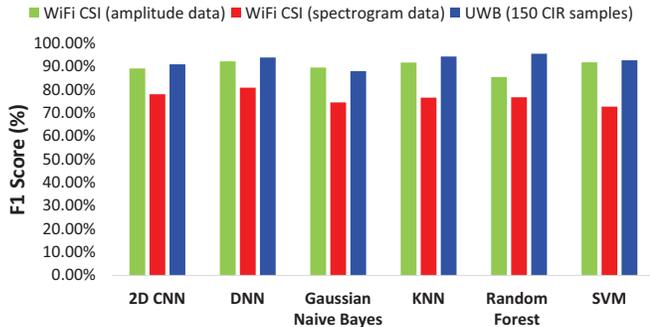

Fig. 8. Performance comparison between WiFi CSI and UWB CIR for HAR.

noticeable variations or patterns in the time domain signal due to human motion. The UWB CIR and WiFi CSI data were collected alongside video recording to obtain ground truth labels. Both the wireless data (UWB and WiFi) and video were timestamped using an external Network Time Protocol (NTP) server for synchronisation purposes.

B. Experimental Results

In this section, we evaluate and compare the performance of the HAR system using UWB CIR and WiFi CSI as features. For this purpose, we considered six classification algorithms, namely, 2D Convolutional Neural Network (CNN), Deep Neural Network (DNN), Gaussian Naive Bayes (GNB), K-Nearest Neighbour (KNN), Random Forest and Support Vector Machine (SVM). The 2D CNN consists of a convolutional layer with 64 filters and 2×2 kernel size and the rectifier (ReLU) as the activation function. The next layer is the max-pooling layer with a stride of 2. The output from the max-pooling layer is then flattened to create a single 1D feature vector. The latter is fed to two fully connected layers (with ReLU activation), the first and second layers consisting of 64 and 32 filters, respectively. Finally, a softmax layer is used for classification of the 5 classes of activities. The DNN consists of 3 fully connected neural network layers with 128, 64 and 16 nodes, respectively. ReLU is used as the activation function in these layers. The output from the third layer is flattened and then fed to a softmax layer for activity classification. For KNN, the number of neighbours was set to 5. A maximum depth of 50 was selected for the Random Forest algorithm while a linear kernel was considered in the SVM algorithm.

80% of the dataset was randomly chosen and used for training while the remaining 20% was used for testing. Fig. 6(a) shows the classification performance of the 6 algorithms when UWB CIR data are used as features. As can be observed,

five out of the six algorithms achieve an F1-score above 90% when only 150 samples are considered in the CIR data as features and used for activity classification. The Random Forest algorithm achieves the highest F1-score at 95.53% while the lowest score is achieved with GNB at 88.04%. The lower score in the GNB case may be attributed to the fact that it assumes feature independence within a class [17], which may not be true in our case. The high score achieved by the Random Forest algorithm may be attributed to its ensemble learning method and its lower susceptibility to over fitting the data even when the number of trees increases.

Fig. 6(b) shows the F1-score comparison when different number of UWB CIR samples are used as features. The F1-scores have been averaged over the 6 classification algorithms and plotted for each number of CIR samples in Fig. 6(b). As can be observed from the latter figure, the highest F1-score is achieved at 92.57% when 150 CIR samples are used as features. However, when 50 and 75 samples are used, the F1-scores are 90.05% and 92.39%, respectively, which are close to the value for the 150 samples case. Therefore, as the number of CIR samples is increased above a certain value, around 75 in this case, there is no major increase in the performance. This means that the rest of the CIR samples do not benefit the machine and deep learning algorithms and can therefore be safely removed when the raw CIR data is denoised. This will further reduce the size of the data and thus the computational complexity is also decreased. From Fig. 6(b), it can also be deduced that using all the 1016 CIR samples (as illustrated in Fig. 1(a)) as features is not beneficial to the classification performance.

Next, we compare the performance of the HAR system when UWB CIR data (150 samples) and WiFi CSI data are used as features. For the WiFi CSI data, we considered two types of feature representations. In the first case, we use the filtered/denoised amplitude values of all 90 subcarriers as features and these are fed to the classification algorithms for performance evaluation. In the second representation, the WiFi CSI data is denoised, reduced in size using PCA and then transformed into spectrograms using STFT, which are then fed to the classification algorithms. Fig. 7 presents spectrograms for the 5 activities. As can be observed in Fig. 7, the activities that involve rapid body motion such as walking have high energy in the higher frequencies in the spectrogram. From Fig. 8, it can be observed that for most classification algorithms, the UWB CIR data (150 samples) achieves better results than WiFi CSI. However, it can also be noticed that the performance with the amplitude WiFi CSI data is very close to the UWB

CIR data. For instance, the amplitude CSI data achieves an F1-score of 92.24% using DNN. The main difference is that the UWB CIR data has a much lower data size than the amplitude WiFi CSI data and still achieves a higher score. As for the case when the CSI spectrograms are used as features, the performance is even lower. For example, a maximum F1-score of 80.89% is achieved using the DNN. The lower scores may be attributed to the fact that when PCA was used for dimensionality reduction, the optimum number of principal components might not have been selected to represent a good variance of the data. Furthermore, in some studies, higher packet rates are used, for example, 2500 packets/s, to capture maximum variations/details in the CSI data caused by human activities of smaller durations [11]. However, this would have resulted in an even larger data size, increasing the computational complexity.

VI. CONCLUSION

The scope of this work was to evaluate the HAR performance in a LoS setup using the high resolution UWB CIR as features. The features were trained using machine/deep learning algorithms to classify five classes of activities including sitting, standing, lying down, standing from the floor and walking. Our results showed that by using CIR samples as features, the five activities could be classified with an F1-score as high as 95.53%. We also evaluated the HAR performance with WiFi CSI data. By considering two types of features for the WiFi CSI data; firstly, denoised amplitude values of 90 subcarriers and secondly, spectrograms obtained from a few principal components, maximum F1-scores of 92.24% and 80.89% were obtained with a DNN, respectively. We can conclude that the UWB technology not only provides a better performance than its WiFi counterpart in terms of HAR but also has several benefits like smaller data dimension and lower signal processing requirement as compared to WiFi systems. In this study it has been shown that, in addition to the primary function of the UWB system which is active localisation, it can also be used as a receiver-only radar system for the passive sensing of human activities.

REFERENCES

[1] H. Thariq, H. Ahmad, and C. Vaithilingam, "Device free human gesture recognition using Wi-Fi CSI: A survey," *Engineering Applications of Artificial Intelligence*, vol. 87, 01 2020.

[2] B. Tan, Q. Chen, K. Chetty, K. Woodbridge, W. Li, and R. Piechocki, "Exploiting WiFi channel state information for residential healthcare informatics," *IEEE Communications Magazine*, vol. 56, no. 5, pp. 130–137, 2018.

[3] C. Rodriguez, D. M. Castro, W. Coral, J. L. Cabra, N. Velasquez, J. Colorado, D. Mendez, and L. C. Trujillo, "IoT system for human activity recognition using bioharness 3 and smartphone," in *Proceedings of the International Conference on Future Networks and Distributed Systems*, ser. ICFNDS '17. New York, NY, USA: Association for Computing Machinery, 2017. [Online]. Available: https://doi.org/10.1145/3102304.3105828

[4] F. Chin-Shyurng, S.-E. Lee, and M.-L. Wu, "Real-time musical conducting gesture recognition based on a dynamic time warping classifier using a single-depth camera," *Applied Sciences*, vol. 9, no. 3, p. 528, 2019.

[5] T. Risset, C. Goursaud, X. Brun, K. Marquet, and F. Meyer, "UWB ranging for rapid movements," in *2018 International Conference on Indoor Positioning and Indoor Navigation (IPIN)*, 2018, pp. 1–8.

[6] H. Abdelnasser, M. Youssef, and K. A. Harras, "WiGest: A ubiquitous WiFi-based gesture recognition system," in *2015 IEEE Conference on Computer Communications (INFOCOM)*, 2015, pp. 1472–1480.

[7] M. J. Bocus, W. Li, J. Paulavicius, R. McConville, R. Santos-Rodriguez, K. Chetty, and R. Piechocki, "Translation resilient opportunistic wifi sensing," in *2020 25th International Conference on Pattern Recognition (ICPR)*, 2020, pp. 5627–5633.

[8] W. Wang, A. X. Liu, M. Shahzad, K. Ling, and S. Lu, "Understanding and modeling of wifi signal based human activity recognition," in *Proceedings of the 21st annual international conference on mobile computing and networking*, 2015, pp. 65–76.

[9] Y. Wang, J. Liu, Y. Chen, M. Gruteser, J. Yang, and H. Liu, "E-Eyes: Device-free location-oriented activity identification using fine-grained WiFi signatures," in *Proceedings of the 20th Annual International Conference on Mobile Computing and Networking*, ser. MobiCom '14. New York, NY, USA: Association for Computing Machinery, 2014, pp. 617–628. [Online]. Available: https://doi.org/10.1145/2639108.2639143

[10] S. Palipana, D. Rojas, P. Agrawal, and D. Pesch, "FallDeFi: Ubiquitous fall detection using commodity wi-fi devices," *Proc. ACM Interact. Mob. Wearable Ubiquitous Technol.*, vol. 1, no. 4, Jan. 2018. [Online]. Available: https://doi.org/10.1145/3161183

[11] W. Wang, A. X. Liu, and M. Shahzad, "Gait recognition using wifi signals," in *Proceedings of the 2016 ACM International Joint Conference on Pervasive and Ubiquitous Computing*, ser. UbiComp '16. New York, NY, USA: Association for Computing Machinery, 2016, pp. 363–373. [Online]. Available: https://doi.org/10.1145/2971648.2971670

[12] S. Tan and J. Yang, "WiFinger: leveraging commodity wifi for fine-grained finger gesture recognition," in *Proceedings of the 17th ACM International Symposium on Mobile Ad Hoc Networking and Computing*, ser. MobiHoc '16. New York, NY, USA: Association for Computing Machinery, 2016, pp. 201–210. [Online]. Available: https://doi.org/10.1145/2942358.2942393

[13] Z. Tian, J. Wang, X. Yang, and M. Zhou, "WiCatch: A wi-fi based hand gesture recognition system," *IEEE Access*, vol. 6, pp. 16 911–16 923, 2018.

[14] Y. Ma, G. Zhou, S. Wang, H. Zhao, and W. Jung, "SignFi: Sign language recognition using wifi," *Proc. ACM Interact. Mob. Wearable Ubiquitous Technol.*, vol. 2, no. 1, Mar. 2018. [Online]. Available: https://doi.org/10.1145/3191755

[15] L. Gong, W. Yang, Z. Zhou, D. Man, H. Cai, X. Zhou, and Z. Yang, "An adaptive wireless passive human detection via fine-grained physical layer information," *Ad Hoc Netw.*, vol. 38, no. C, pp. 38–50, Mar. 2016.

[16] S. Liu, Y. Zhao, F. Xue, B. Chen, and X. Chen, "DeepCount: Crowd counting with WiFi via deep learning," 2019.

[17] S. Sharma, H. Mohammadmoradi, M. Heydariaan, and O. Gnawali, "Device-free activity recognition using ultra-wideband radios," in *2019 International Conference on Computing, Networking and Communications (ICNC)*, 2019, pp. 1029–1033.

[18] "Dw1000 user manual," https://www.decawave.com/dw1000/usermanual/, (Accessed on 02/02/2021).

[19] P. Corbaln and G. P. Picco, "Ultra-wideband concurrent ranging," 2020.

[20] D. Halperin, W. Hu, A. Sheth, and D. Wetherall, "Tool release: Gathering 802.11 n traces with channel state information," *ACM SIGCOMM Computer Communication Review*, vol. 41, no. 1, pp. 53–53, 2011. [Online]. Available: https://dhalperi.github.io/linux-80211n-csitool/

[21] Z. Dong, F. Li, J. Ying, and K. Pahlavan, "Indoor motion detection using Wi-Fi channel state information in flat floor environments versus in staircase environments," in *Sensors*, 2018.

[22] W. Wang, A. X. Liu, M. Shahzad, K. Ling, and S. Lu, "Device-free human activity recognition using commercial wifi devices," *IEEE Journal on Selected Areas in Communications*, vol. 35, no. 5, pp. 1118–1131, 2017.